

Effects of Precipitation on Sonic Anemometer Measurements of Turbulent Fluxes in the Atmospheric Surface Layer

ZHANG Rongwang¹⁾, HUANG Jian²⁾, WANG Xin³⁾,*, ZHANG Jun A.⁴⁾,
and HUANG Fei^{1),2)}

1) *Physical Oceanography Laboratory/Qingdao Collaborative Innovation Center of Marine Science and Technology, Ocean University of China, Qingdao 266100, P. R. China*

2) *Joint Open Laboratory of Marine Meteorology (JOLMM), Guangzhou Institute of Tropical and Marine Meteorology, CMA, Guangzhou 510080, P. R. China*

3) *State Key Laboratory of Tropical Oceanography (LTO), South China Sea Institute of Oceanology, Chinese Academy of Sciences, Guangzhou 510301, P. R. China*

4) *Rosenstiel School of Marine and Atmospheric Science, University of Miami, FL 33124, USA*

(Received November 18, 2014; revised January 4, 2015; accepted January 5, 2016)

© Ocean University of China, Science Press and Springer-Verlag Berlin Heidelberg 2016

Abstract Effects caused by precipitation on the measurements of three-dimensional sonic anemometer are analyzed based on a field observational experiment conducted in Maoming, Guangdong Province, China. Obvious fluctuations induced by precipitation are observed for the outputs of sonic anemometer-derived temperature and wind velocity components. A technique of turbulence spectra and cospectra normalized in the framework of similarity theory is utilized to validate the measured variables and calculated fluxes. It is found that the sensitivity of sonic anemometer-derived temperature to precipitation is significant, compared with that of the wind velocity components. The spectra of wind velocity and cospectra of momentum flux resemble the standard universal shape with the slopes of the spectra and cospectra at the inertial subrange, following the $-2/3$ and $-4/3$ power law, respectively, even under the condition of heavy rain. Contaminated by precipitation, however, the spectra of temperature and cospectra of sensible heat flux do not exhibit a universal shape and have obvious frequency loss at the inertial subrange. From the physical structure and working principle of sonic anemometer, a possible explanation is proposed to describe this difference, which is found to be related to the variations of precipitation particles. Corrections for errors of sonic anemometer-derived temperature under precipitation is needed, which is still under exploration.

Key words precipitation; sonic anemometer; virtual temperature; turbulent flux; spectra

1 Introduction

Field observation of turbulent flows in the atmospheric boundary layer and/or surface layer, requires instruments that have the ability to simultaneously detect fluctuations of wind and temperature and other variables. The sonic anemometer has been extensively applied in previous field experiments to measure turbulent fluxes owing to its advantages of ultrasonic signal (Kaimal and Businger, 1963; Kaimal *et al.*, 1990; Friebel *et al.*, 2009; Kochendorfer *et al.*, 2012; Frank *et al.*, 2013). Barret and Suomi (1949) designed a pioneer sonic anemometer and described its principle that the transit time of sound pulses in air is computed to derive values related to wind and temperature. Corby (1950) and Schotland (1955) designed the anemometers that employ an acoustic source and four

receivers all in one plane. Kaimal and Businger (1963) began to use continuous sound signals instead of sound pulses, which promoted the anemometer system to perform more stably and less noisily. Both tower sites (Dabberdt, 1968; Grelle and Lindroth, 1994; Liu *et al.*, 2001) and research aircrafts (Vellinga *et al.*, 2013) began to use sonic anemometers as fundamental instruments for detailed studies of the atmospheric surface layer.

Despite that sonic anemometers have inherent advantages in measuring high-frequency signals of turbulent flows, they are prone to produce errors when influenced by internal/external factors (Moore, 1986; Kraan and Oost, 1989; Larsen *et al.*, 1993). For instance, sonic anemometers usually suffer the transducer-shadow effect (Wyngaard, 1981; Wyngaard and Zhang, 1985; Grant and Watkins, 1989). The flow distortion (Britter *et al.*, 1979) caused by such effect substantially leads to underestimate of wind velocity (Kaimal *et al.*, 1990). A theoretical model that used to partially eliminate the effect of flow distortion was suggested by Wyngaard (1981). Wyngaard

* Corresponding author. Tel: 0086-20-34134191

E-mail: wangxin@scsio.ac.cn

and Zhang (1985) declared that optimum designs for sensors seem to preferably minimize their shadow effects and compensate the uncertainties in the data analysis. Analyzing data collected during the 1968 Kansas field experiment, Friehe (1976) discussed the effects of sound speed fluctuations on sonic anemometer measurements and provided a series of correction algorithms. By employing the simultaneous observation from a sonic anemometer, a Lyman- α hygrometer and a fast response thermocouple, Schotanus *et al.* (1983) assessed the errors of the sonic anemometer for measuring temperature variance and turbulent flux and proposed expressions for correcting them. Recently, Burns *et al.* (2012) showed that the error of sensible heat flux calculated from measurements of sonic anemometer tends to be enlarged with an increasing wind velocity, which could be connected with the shake of sensors caused by strong wind. Nakai and Shimoyama (2012) made a detailed analysis for the errors caused by the angle of attack, which tended to result in the increase of eddy flux.

With the development of improved structure of sensor geometries and technologies for implemented online calibrations, modernized three-dimensional sonic anemometers enhance the accuracy and precision of measurements (Wieser *et al.*, 2001; Cuerva *et al.*, 2004). Recently developed state-of-the-art commercial sonic anemometer has been alleged to withstand the impact of precipitation to some degree. For example, the WindMaster Pro of Gill Instruments explicitly identifies in the product manual that it bears rain rate up to 300 mm h^{-1} . Nevertheless, the sensors of the sonic anemometer are sensitive to impurities, such as the raindrop (van Boxel *et al.*, 2004). In previous studies, data collected during precipitation are generally removed to adequately guarantee the quality controls. It is negligible to discard those suspicious measurements in a relatively long-term series of datasets, but unadvisable to the research of synoptic scale such as sea fog and tropical cyclones. Since humidity is usually large and precipitation happens frequently in such conditions, it is crucial to understand the effect of precipitation on the flux measurements using sonic anemometers.

The objective of this paper is to investigate effects of precipitation on sonic anemometer measurements of turbulent fluxes in the atmospheric surface layer. During the field observational experiment, a heavy rain event was recorded continuously with synchronous measurements of

wind and temperature and information of the precipitation, features of which are subsequently discussed from the perspective of statistics and in the framework of similarity theory. Our long-term goal is to provide possible references for selecting and calibrating measurements during different weather background henceforward. In Section 2, the fundamental information of the field observation experiment is introduced. In Section 3, the main results of measurements are showed. Conduction and discussion are given in Section 4.

2 Description of Field Experiment and Analysis Method

The field experiment, from May 15 to 22 in 2013, was conducted in the Marine Meteorological Science Experiment Base (MMSEB) at Bohe, Maoming, Guangdong Province, China ($21^{\circ}27'37''\text{N}$, $111^{\circ}19'24''\text{E}$). The location of MMSEB is shown in Fig.1, which is on the relatively flat coastline of a peninsula with surroundings of complicated terrains.

The sonic anemometer, WindMaster Pro, produced by the Gill Instruments, was used in our experiment. Details of the anemometer are listed in Table 1. The WindMaster Pro (Fig.2) is built using stainless steel which can survive

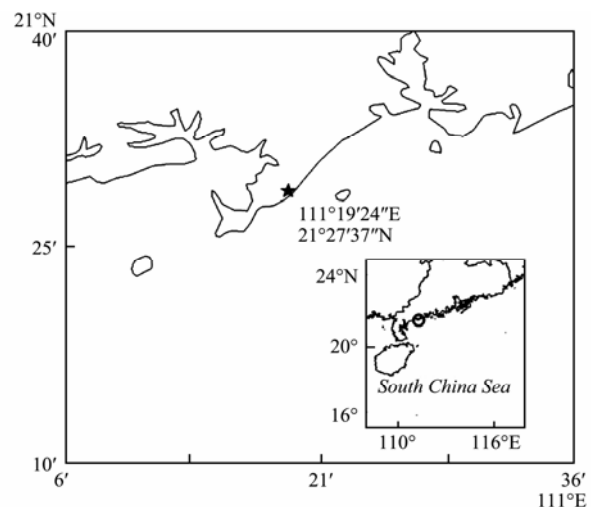


Fig.1 The map of Bohe observation site in Maoming, Guangdong Province, China. The black pentagram denotes the exact location where field experiment was conducted.

Table 1 Main parameters of WindMaster Pro

Parameter	Values	Parameter	Values
Sample rate	32 Hz	Output rate	1, 2, 4, 8, 10, 16, 20, 32 Hz
Wind speed range	$0-65 \text{ m s}^{-1}$	Wind speed resolution	0.01 or 0.001 m s^{-1}
Wind direction range	$0-359.9^{\circ}$	Wind direction resolution	1° or 0.1°
Sound speed range	$300-370 \text{ m s}^{-1}$	Sound speed resolution	0.01 m s^{-1}
Sonic temperature range	-40 to 70°C	Sonic temperature resolution	0.01°C
Operating temperature	-40 to 70°C	Humidity	$<5\%$ to 100%
Weight	1.7 kg	Size	$750 \text{ mm} \times 240 \text{ mm}$
Power requirement	9-30 V DC	Digital output protocol	RS232, RS422, RS485
Baud rates	2400-57600	Precipitation	300 mm h^{-1}

Note: The data are derived from the user manual of WindMater Pro at the website of Gill Instruments Ltd. (www.gillinstruments.com/data/manuals/WindMaster-and-Windmaster-Pro-Manual.pdf).

conditions with a maximum operating wind speed of 65 m s⁻¹. With a maximum data output rate of 32 Hz as standard, improved vertical resolution and sound speed accuracy and less distortion due to wind loading, this kind of three-dimensional anemometer is particularly suitable for precise wind measurements.

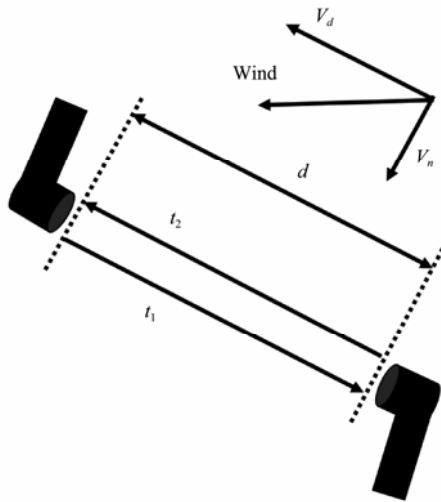


Fig.2 Schematic drawing of WindMaster Pro, where d is the length between emitting and receiving transducers, t_1 and t_2 the transmitting time of ultrasonic signal along and against the wind, respectively, V_d and V_n the components of wind along and perpendicular to the signal path respectively. The WindMaster Pro is mounted at the altitude of 3 m.

The sonic anemometer determines the wind velocity components and sound speed by measuring the transit times of sound pulses traveling in two opposite directions along each of the three acoustic paths. From the schematic drawing in Fig.2, the transit time of t_1 against the wind direction and t_2 along the wind direction can be expressed as

$$t_1 = \frac{d}{c - V_d}, \tag{1a}$$

$$t_2 = \frac{d}{c + V_d}, \tag{1b}$$

where d is the length of acoustic path, c the sound speed, V_d the wind component that along each pair of transducers.

Then t_1 and t_2 can be combined to get

$$V_d = \frac{d}{2} \left(\frac{1}{t_2} - \frac{1}{t_1} \right), \tag{2a}$$

$$c = \frac{d}{2} \left(\frac{1}{t_2} + \frac{1}{t_1} \right). \tag{2b}$$

The wind components are calculated along three axes, which are then transformed to the horizontal winds u and v and vertical wind w , according to internal rotation matrix of the sonic anemometer. The sound speed is averaged with three measurements along each axis, which

depends on air density and is influenced by air temperature, therefore serving as an indicator of air temperature. Particularly, sonic anemometer-derived temperature is referred to as the sonic virtual temperature but not exactly the same as the virtual temperature, despite that the difference between them is substantially negligible (van Boxel *et al.*, 2004). Given that the sound speed and sonic virtual temperature are related to each other (Kaimal and Businger, 1963), the sonic virtual temperature can be estimated as

$$T_s = \frac{c^2}{\gamma_d R_d} = T(1 + 0.317e/P) = T(1 + 0.51q), \tag{3}$$

where T_s is the sonic virtual temperature, γ_d the ratio of dry air specific heat at constant pressure to specific heat at constant volume, R_d the dry air gas constant, T the air temperature, e the vapor pressure, P the air pressure, and q the specific humidity. Note that the wind velocity components and sound speed are originally determined by the transit time, thus are independent of temperature, humidity, pressure or precipitation and so on.

In the vicinity of WindMaster Pro, an optical rain gauge (ORG) and a disdrometer named Parsivel were mounted to measure the synchronous information of precipitation. The most obvious difference between these two instruments is that ORG is based on infrared technique while the Parsivel based on laser. Fig.3 shows a comparison of rain rate records from ORG and Parsivel from a selected observational period indicating good agreement. During this period, the accumulated precipitation of 9.07 mm was recorded by both instruments. This result provides us confidence in the precipitation measurements.

In the atmospheric surface layer, turbulent fluxes of momentum and sensible heat are generally calculated with the eddy correlation method (Swinbank, 1951):

$$\tau = \rho (\overline{u'w'^2} + \overline{v'w'^2})^{1/2}, \tag{4}$$

$$H = \rho c_p \overline{w'\theta'}, \tag{5}$$

where τ and H are the momentum and sensible heat flux respectively; u , v and w the along-wind velocity, cross-wind velocity and vertical velocity respectively; ρ the air density, c_p the specific heat at constant pressure, and θ the potential temperature. The prime represents turbulent fluctuations and an overbar denotes averages over the flux run. The scaling parameters are defined as

$$u_* = (\overline{u'w'^2} + \overline{v'w'^2})^{1/2} = (\tau / \rho)^{1/2}, \tag{6}$$

$$\theta_* = -\overline{w'\theta'} / u_* = -H / \rho c_p u_*, \tag{7}$$

where u_* and θ_* are the scaling parameters for wind and temperature, respectively. In the framework of Monin-Obukhov similarity theory (Monin and Obukhov, 1954), the behavior of spectra and cospectra of turbulence in the surface layer are expected to be reduced to some univer-

sal shapes with appropriate manner of normalization (Kaimal *et al.*, 1972; Horst and Oncley, 2006; Zhang, 2010). According to the methods indicated by Kaimal *et al.* (1972), the spectra density of velocity in the inertial subrange can be normalized to the form

$$\frac{fS(f)}{u_*^2} = \frac{\alpha}{(2\pi k)^{2/3}} \phi_\varepsilon^{2/3} n^{-2/3}, \quad (8)$$

where f is the frequency, $S(f)$ the spectra density computed with the fast Fourier transform, $n=fz/U$ the dimen-

sionless frequency (z the instrument height, U the mean wind velocity), u_* the friction velocity, α the universal parameter, k the von Karman parameter, and ϕ_ε the dimensionless dissipation. Generally, temperature spectra are very close to velocity spectra, with an identical power $-2/3$. For cospectra, similar expressions are derived except for a power $-4/3$. With the highlighted characteristics of the normalized spectra and cospectra, it is efficient and executable to compare the spectra and cospectra of measurements to the standard ones in order to validate their availability.

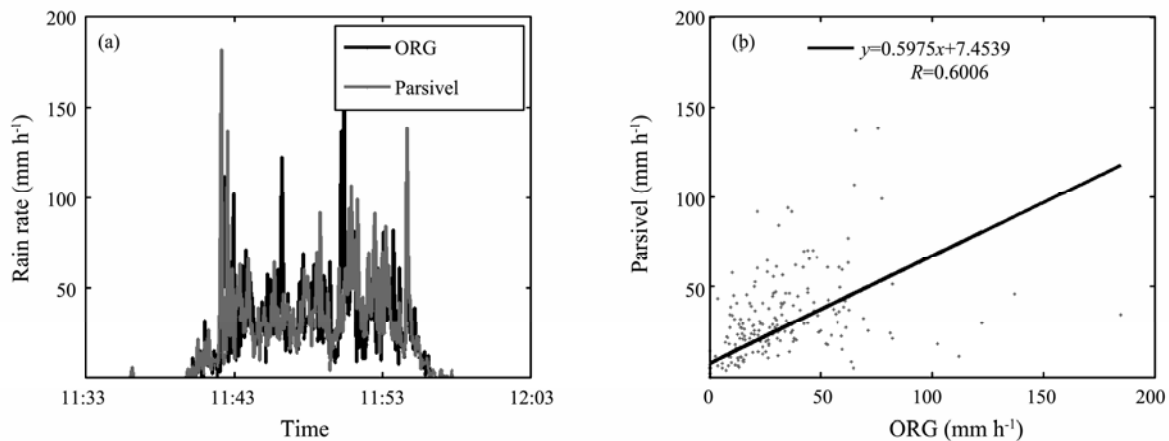


Fig.3 Rain rate measurements from ORG and Parsivel: (a) raw 0.2Hz data; (b) linear least square fitting between data from ORG and Parsivel.

3 Results

3.1 Measurements of Sonic Anemometer

To investigate the effects of precipitation on sonic anemometer measurements of fluxes and spectra, we focused on the data from local time 10:00 to 16:00 on March 19, 2013. During this period, the mean wind speed was 2.4 m s^{-1} . The period from 11:33 to 12:03 encountered a heavy rainfall with an 8.84 mm of accumulated precipitation being recorded.

The raw 20Hz horizontal wind velocity with 1-minute averages are depicted in Fig.4a, showing that the measured wind speeds are $<10 \text{ m s}^{-1}$ throughout the focused period. The wind direction was mainly from the east, indicating that the winds blew from the ocean. When precipitation occurred, there are evident fluctuations of wind velocity but in a relatively small range. The sonic virtual temperature T_s and turbulent wind velocity components u , v , w are shown in Fig.5 with raw 20Hz data and fluctuations from the 1-minute mean. In the raw data and fluctuations, wind velocity components exhibit no significant variations before or after precipitation. However, the sonic virtual temperature T_s presents large sensitivity to the precipitation. Before the precipitation occurs, the raw data of T_s (Fig.5a) show a decreasing trend and the fluctuations of T_s (Fig.5b) are quite stable. However, the raw data turn to rise sharply and the amplitude of fluctuations also increased rapidly from the beginning of

precipitation. When the precipitation disappears, these variations gradually drop to its previous level about 1 hour later.

The 10-minute standard deviations (STD) of u , v , w and T_s during the observation period are shown in Fig.6. All the shapes of STDs of u , v , w are extremely similar, indicating that the airflow is isotropic. From 11:33 on, all of the STDs turn to rise up at the moment of the occurrence of precipitation. But be careful, this change about 1 m s^{-1} for wind velocity is not surprisingly large when compared with 1°C for temperature, since wind speed varies more quickly than air temperature. STD of T_s jumps the most significantly, due to the notable sensitivity of T_s to precipitation, which increases 5 times of the ones before precipitation. When precipitation disappears, the STDs turn to fall back to relatively stable state as the previous level without precipitation. It is noteworthy that suspiciously high STDs of T_s emerges around 10:19 when a small amount of precipitable particles are detected by both ORG and Parsivel, which provides an additional verification that the sonic anemometer-derived temperature is sensitive to precipitation.

3.2 Spectra and Cospectra Characteristics

The normalized spectra of u , v , w and T_s are depicted in Figs.7a–d, in which each curve denotes spectra or cospectra density computed using data every 30-minute centered at the time of high precipitation. All of the normalized spectra of u , v , w are grouped into a family of

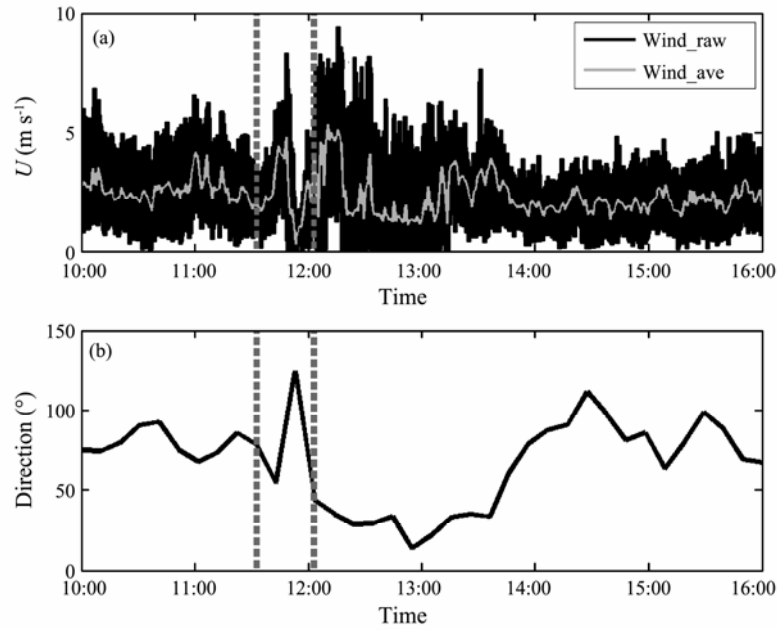


Fig.4 Variations of (a) horizontal wind velocity U and (b) horizontal wind direction during the observational period. Black and gray curves denote the raw 20Hz data and the 1-minute averaged results, respectively. For wind direction, 0° means the northern wind. The vertical gray dotted lines in both panels denote the period of precipitation.

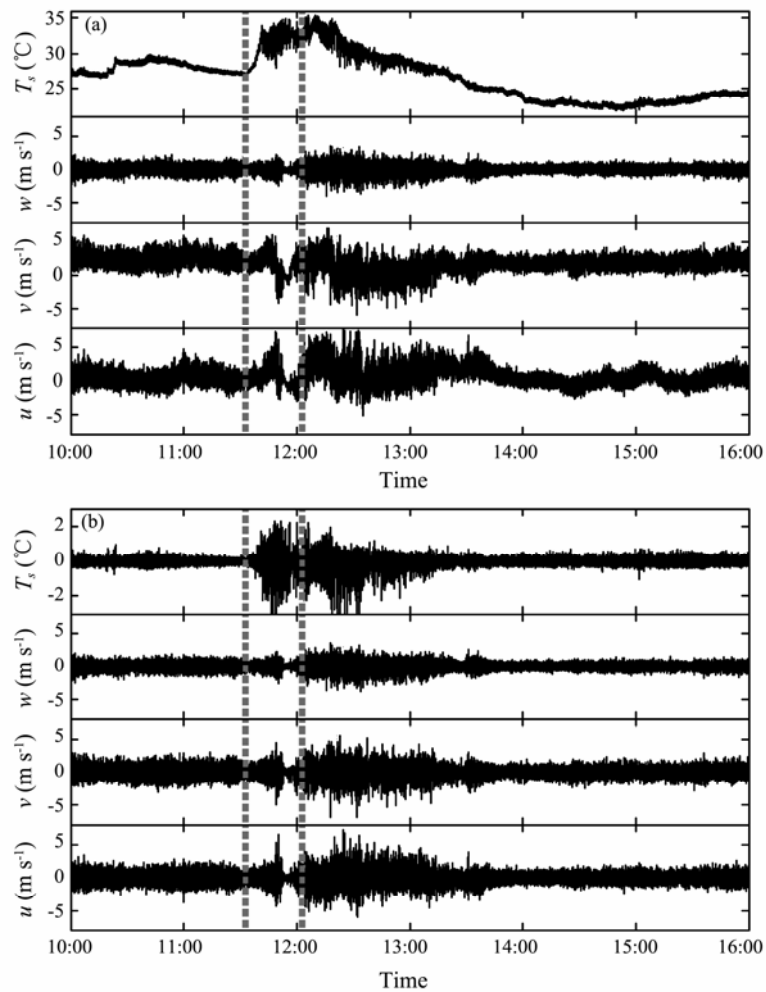


Fig.5 Variation of (a) raw 20Hz data and (b) fluctuations of wind components and sonic temperature measured by WindMaster Pro. The fluctuation is defined as the raw data minus their mean values in every minute. The vertical gray dotted lines denote the period of precipitation.

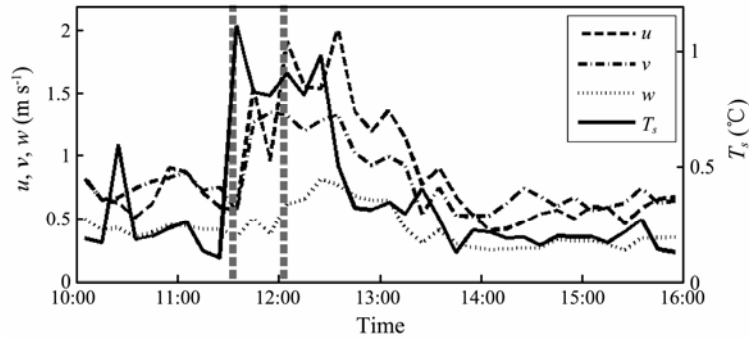


Fig.6 Standard deviation of wind components u (dashed line), v (dashed-dotted line), w (dotted line) by the left axis and sonic virtual temperature T_s (solid line) by the right axis. All the STDs are calculated in each non-overlapping 10 minutes with 12000 points. The vertical gray dotted lines denote the period of precipitation.

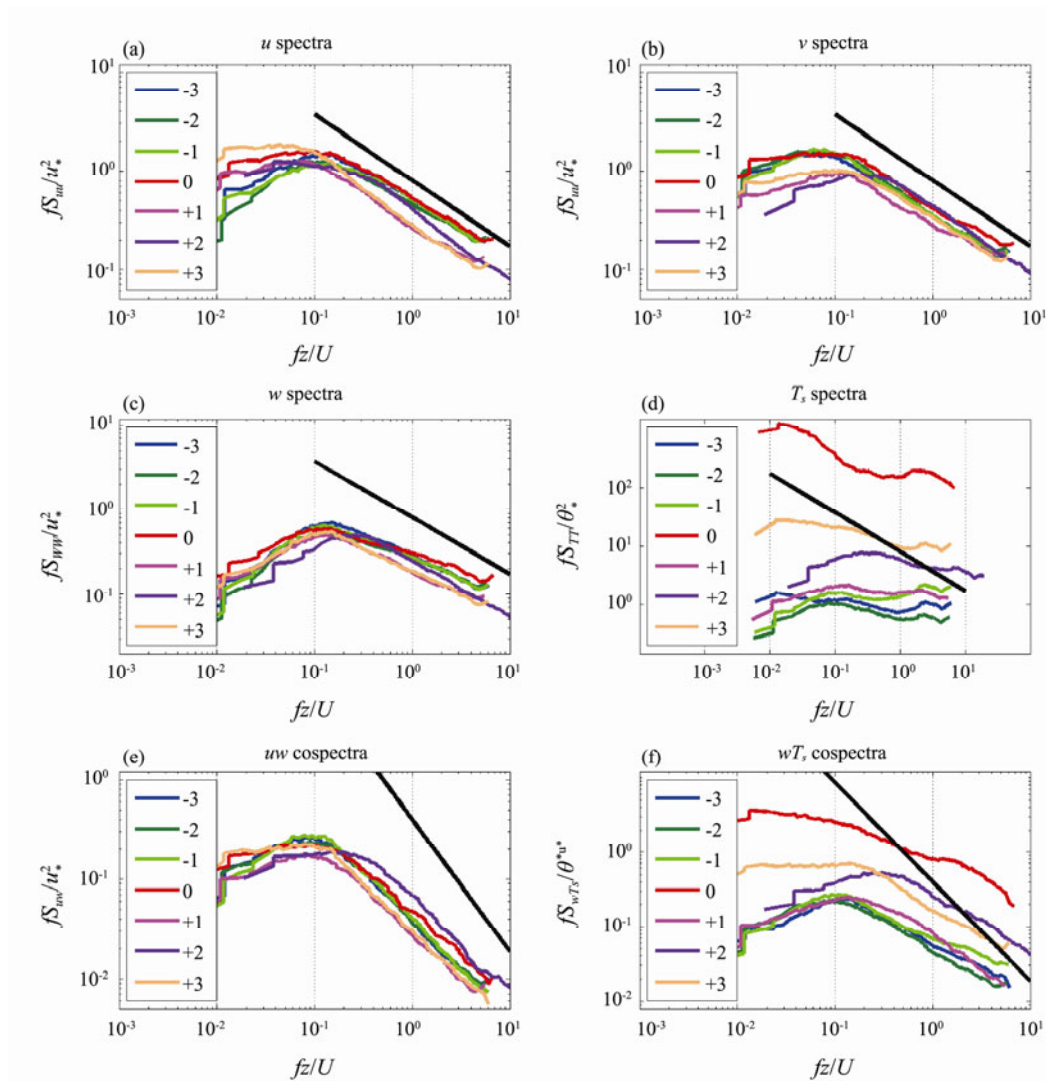


Fig.7 Normalized spectra and cospectra in every 30-minute run. (a)–(d) are the spectra of u , v , w and T_s , respectively. (e) and (f) are the cospectra of uw and wT_s , respectively. Numbers from ‘-3’ to ‘+3’ refer to the 30-minute time slices. ‘0’ means the rainfall time of 11:34–12:03. ‘-3’, ‘-2’, and ‘-1’ mean 10:04–10:33, 10:34–11:03, and 11:04–11:33, which are before rainfall time. ‘+1’, ‘+2’ and ‘+3’ mean 12:04–12:33, 12:34–13:03, and 13:04–13:33, which are after rainfall time. The black thick line denotes the reference slope $-2/3$ in (a)–(d) and $-4/3$ in (e) and (f).

well-defined curves with a slope very close to $-2/3$ in the inertial subrange, suggesting that the precipitation has no obvious effects on measurements of wind velocity. It also indicates that the turbulent flow systematically follows

the similarity theory in our field observational experiment. The spectra of T_s , however, is distinctly scattered, especially during the precipitation, which can not be sorted into a universal shape. The spectra density increases by

two orders of magnitude when the precipitation occurs, implying that the suddenly rising of fluctuations of sonic virtual temperature is probably abnormal as a consequence of precipitation effect. Notably, almost all of the normalized curves of T show a smaller slope than $-2/3$ in the inertial subrange, suggesting that frequency loss exists all the time. Precipitation and high humidity likely contaminate sonic anemometer temperature measurements. Furthermore, upwarping in the high frequency part (1–10 Hz) in the spectra of T_s is obvious, which may be involved with the inadequate sampling rate or interference of high frequency noise.

The normalized cospectra of uw , which are proportional to momentum fluxes, exhibit no abnormality and the curves are grouped into shapes with a slope close to $-4/3$ in the inertial subrange (Fig. 7e). This suggests that the momentum flux is little influenced by precipitation. Note that our results for spectra of wind velocities and cospectra of momentum flux are consistent with those given by Kaimal *et al.* (1972) and Zhang (2010). Nevertheless, the normalized cospectra of wT_s , which is proportional to sensible heat flux, have slopes less than $-4/3$ mainly due to the influenced T_s by precipitation (Fig. 7f). It suggests that the uncertainty of the measured sensible heat flux is significant around the period which contains precipitation.

3.3 Error Analysis

The preceding analysis mentioned that T_s is sensitive to precipitation. From the view of spectra and cospectra, it implies that the rising up of mean values and fluctuations of T_s during precipitation are irrational. According to expression (3), T_s is determined by both air temperature and humidity. The differences between air temperature and sonic virtual temperature are estimated assuming that the water vapor is saturated all the time (Fig. 8), which denotes the greatest contribution of water vapor to T_s . It is found that the differences monotonically increase with air temperature but never exceed 0.6°C in the range of 27– 34°C . Although the occurrence of precipitation gives rise to a high or even saturated air humidity, it can not explain the remarkable rising of T_s , which increases by 7°C in as short as 7 minutes at the beginning of precipitation (Fig. 5a). Then the question goes to if the rising of T_s is the result of increasing in air temperature. When precipitation occurs, taking into account the heat absorbed by water evaporation, the environmental temperature trends to decline slightly. Even assuming that local heating can be induced by horizontal advection, it is hard to expect a significant rising of T_s in conditions where the horizontal wind changes little and the sonic virtual temperature keeps a decreasing trend before precipitation. Because of lack of synchronous observations of air temperature and water vapor near the sonic anemometer, it is of serious difficulty to understand the true variabilities of sonic virtual temperature during precipitation. Fortunately, the measurements from a thermometer/hygrometer called HMP45 of the Vaisala company, although deployed not

collocated with but relatively close to the sonic anemometer, can help us qualitatively verify the trend of air temperature around the period of precipitation. The measurements from HMP45 (defined as T) are used as an indicator of the true trend of air temperature variations, regardless of its systematic errors. It is found that T_s and T vary with a similar trend most of the time without precipitation (Figs. 9a, b, e). The air temperature experiencing a decrease with time during the precipitation from HMP45 confirms that the rising of T_s during precipitation (Fig. 9c) is abnormal. At the end of precipitation, T_s is still affected but begins to go down gradually, with the trends of T_s and T continually being in opposite directions (Fig. 9d). Once the effect of precipitation weakens to a certain degree, T_s resumes to vary with the same trend as T .

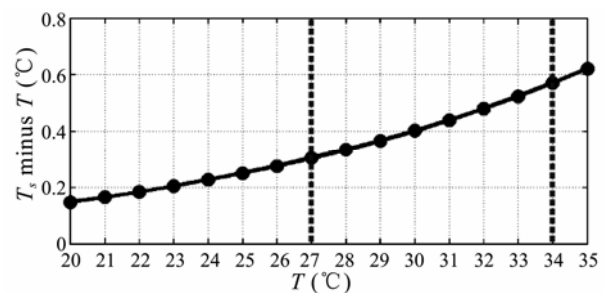


Fig. 8 Estimation of the difference between virtual temperature (T_s) and air temperature (T) for saturated moisture. The vertical gray dotted lines denote the range of virtual temperature measured around the period of precipitation.

It is inferred from above that the rising of precipitation-affected sonic virtual temperature is hardly induced by water vapor or air temperature. A possible explanation is proposed through the principle of the sonic anemometer. Due to the medium between the pair of sonic sensors changes from dry air to wet air with liquid water, the speed of sound will be accelerated since sound propagates faster in water than in gas, which results in decreased transit time of t_1 and t_2 in expression (1). When smaller t_1 and t_2 become reciprocals in expression (2b), a larger sound speed c is derived. The expression (3) when applied in condition of dry or wet air seems to have deficiency in transforming the sound speed to sonic virtual temperature when liquid water enters, which can cause irrational high values of T_s rising from the high sound speed values. On the contrary, wind velocity components are direct output from expression (2a), and are calculated with the difference of the reciprocals of t_1 and t_2 , thus are less contaminated by the shortened transit time due to precipitation.

4 Conclusion and Discussion

In this study, the effects of precipitation on sonic anemometer measurements are examined in the framework of similarity theory using data collected during the field experiment conducted at MMSEB. It is found that the

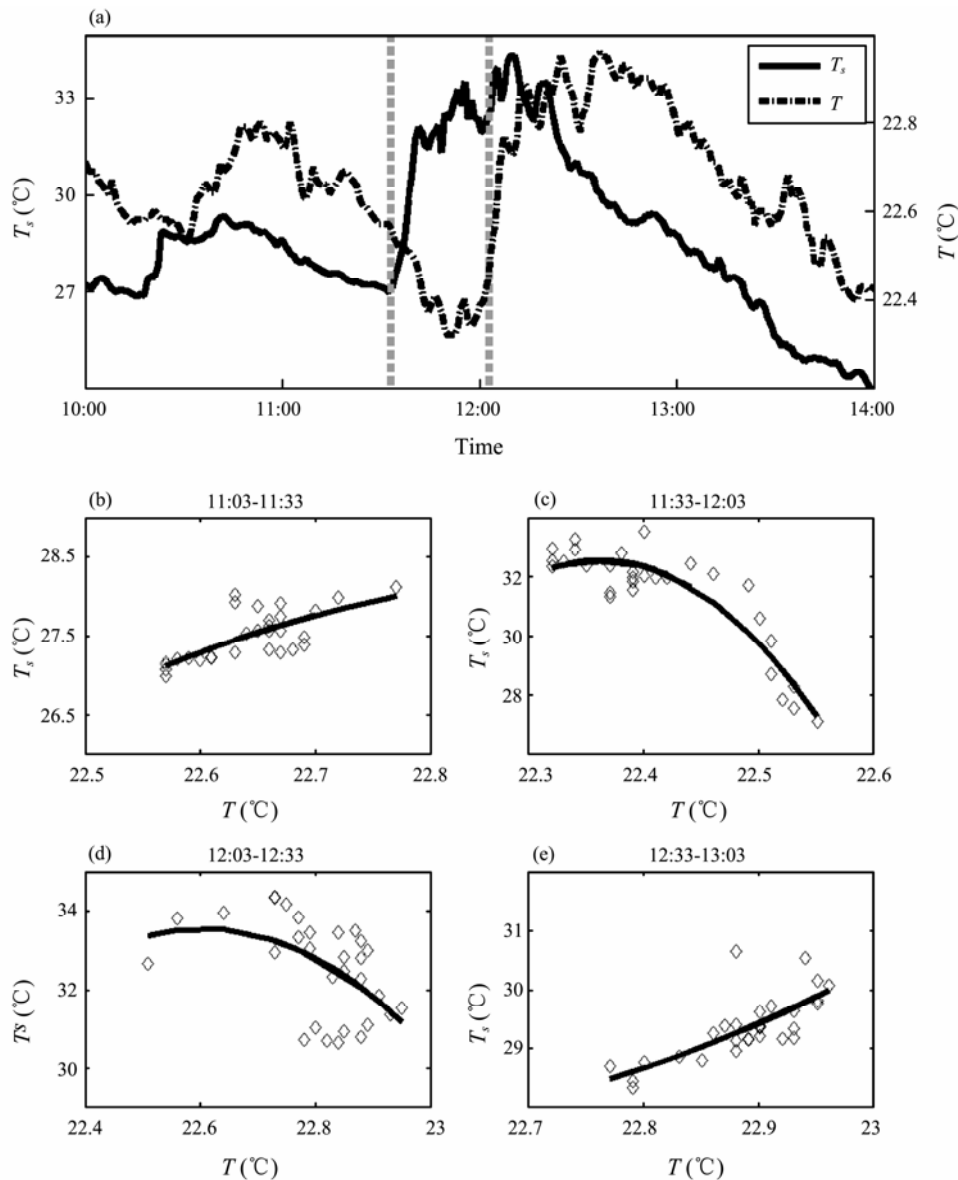


Fig.9 (a) Variations of sonic virtual temperature (solid line) and air temperature (dotted-dashed line); (b)–(e) are scatter diagrams of air temperature and sonic virtual temperature from 11:03 to 13:03 per 30 minutes. Solid black lines denote the quadratic polynomial fitting results.

wind velocity components of sonic anemometer are not affected by the precipitation. The sonic virtual temperature, however, presents remarkable errors due to the effects of precipitation. The turbulence spectra and cospectra are utilized to validate the quality of flux measurements from sonic anemometer. The normalized spectra of wind velocities fall into uniform shapes with the standard slope of $-2/3$ in the inertial subrange. The cospectra of uw also fall into the universal shape with the standard slope of $-4/3$ in the inertial subrange. This result suggests that the wind velocity components and associated momentum flux present reliable resistance to the precipitation. However, the spectra of temperature and cospectra of sensible heat flux do not exhibit a universal shape and have obvious frequency loss during precipitation.

The working principle of sonic anemometer helps understand the possible reasons that cause errors in sonic virtual temperature. When the medium between the pair

of sonic sensors changes from air to air with liquid water, the transit time becomes shortened and results in a higher calculated sound speed with expression (2b). Subsequently, through the transformation of expression (3), the sonic virtual temperature is amplified. It is obvious that expression (3) applicable in condition of dry or wet air seems to have deficiency in that of precipitation. Under this explanation, variations of sonic virtual temperature are possibly related to the characteristics of precipitation.

The sonic virtual temperature goes up sharply at the moment of precipitation and falls down when the precipitation disappears, which is somewhat consistent with the variation of rain particle numbers. Fig.10 shows the relationship between sonic virtual temperature and precipitation particle number. In the first 8 minutes of the precipitation, a positive relationship is distinct with a correlation coefficient up to 0.8, which, however, weakens to -0.22 in the subsequent 22 minutes (Fig.10b). What causes the

difference between these two periods? Fig.10c shows the raindrop size distribution during the precipitation. At the beginning of the precipitation, the raindrops with larger size increases rapidly, which then break into massive smaller particles. This process possibly causes the medium between sonic sensors to be strongly disturbed, which, as mentioned before, affects the measurements of sonic virtual temperature eventually. That is why the re-

markable change of relationship occurs in the two periods. When the characteristics of particles become relatively stable, the medium tends to suffer fewer disturbances than in the first period, indicating a weakened influence of precipitation on sonic virtual temperature. Since the sensors of the sonic anemometer get wet after the precipitation ceases, the influence continues to exist for a certain period (Fig.9d).

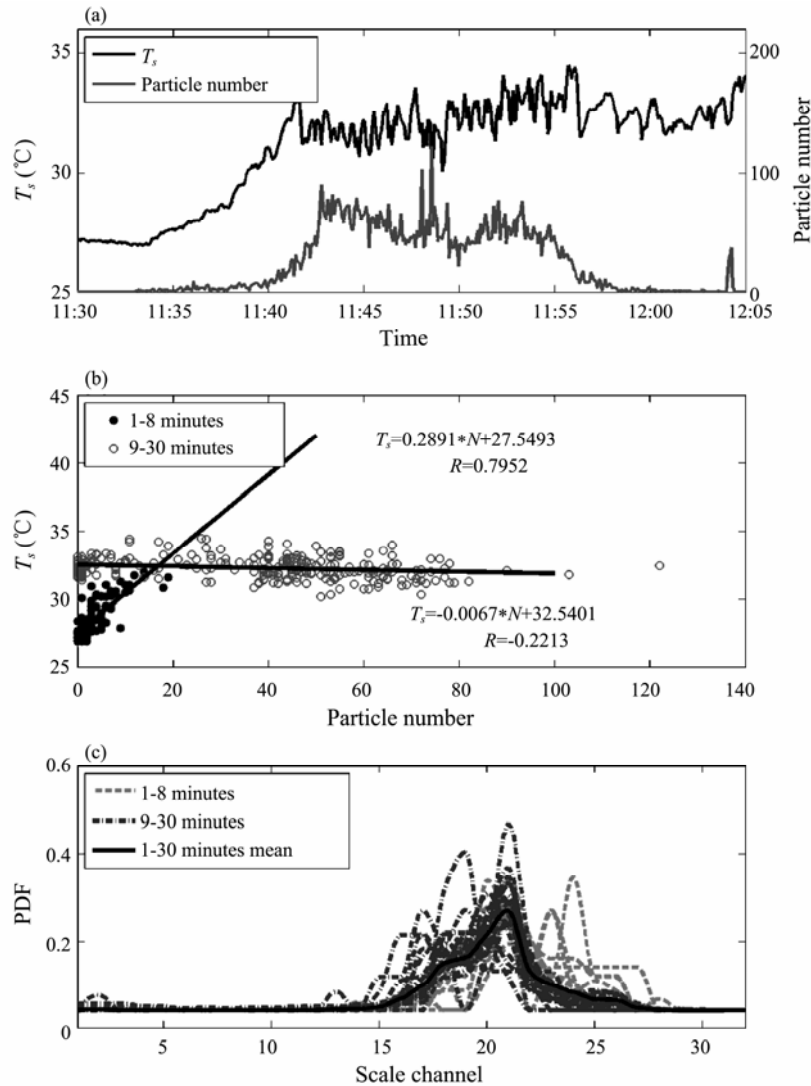


Fig.10 (a) sonic virtual temperature (black curve) and rain particle number (gray curve) per 5 second during raining time; (b) the scatter diagram of particle number and sonic virtual temperature, where black dots denote the data of 1–8 minutes and gray circles the data of 9–30 minutes. The black solid lines denote the linear least square fitting. (c) raindrop size distribution. The scale channel is related to the raindrop diameter with lower values for smaller diameter and higher values for larger ones. The PDF refers to the probability distribution function. The dashed light gray curves denote the data of 1–8 minutes, dot-dashed dark gray curves 9–30 minutes, and thick black curve mean values of 1–30 minutes.

This paper highlights the characteristics of wind and temperature measurements from the sonic anemometer under precipitation conditions. It is believed that our results will lead to better understanding of the performance of sonic anemometer. Corrections for sonic anemometer-derived temperature are recommended before flux calculation under precipitation based on our results. Such correction will improve the quality of observed sensible heat fluxes based on eddy covariance method, especially

in severe weather conditions such as tropical cyclones. Future work will focus on methods to correct precipitation-contaminated temperature observations by sonic anemometers.

Acknowledgements

This work was supported by the National Key Basic Research Program of China (Grant Nos. 2014CB953903,

2015CB953904), the Strategic Priority Research Program of the Chinese Academy of Sciences (Grant No. XDA 11010403) and the CAS/SAFEA International Partnership Program for Creative Research Teams. The data was provided by the Bohe Marine Meteorological Science Experiment Base, Guangzhou Institute of Tropical and Marine Meteorology, CMA.

References

- Barret, E. W., and Suomi, V. E., 1949. Preliminary report on temperature measurements by sonic means. *Journal of Meteorology*, **6**: 273-276.
- Britter, R. E., Hunt, J. C. R., and Mumford, J. C., 1979. The distortion of turbulence by a circular cylinder. *Journal of Fluid Mechanics*, **92**: 269-301.
- Burns, S. P., Horst, T. W., Blanken, P. D., and Monson, R. K., 2012. Using sonic anemometer temperature to measure sensible heat flux in strong winds. *Atmospheric Measurement Techniques*, **5**: 447-469.
- Corby, R. E., 1950. Acoustic anemometer-anemoscope. *Electronics*, **1**: 88-90.
- Cuerva, A., Andrés, A. S., and López, O., 2004. Singularities and undefinitions in the calibration functions of sonic anemometers. *Journal of Atmospheric and Oceanic Technology*, **21**: 1868-1875.
- Dabberdt, W. F., 1968. Tower-induced errors in wind profile measurements. *Journal of Applied Meteorology*, **7**: 359-366.
- Frank, J. M., Massman, W. J., and Ewers, B. E., 2013. Underestimates of sensible heat flux due to vertical velocity measurement errors in non-orthogonal sonic anemometers. *Agricultural and Forest Meteorology*, **171-172**: 72-81.
- Friebel, H. C., Herrington, T. O., and Benilov, A. Y., 2009. Evaluation of the flow distortion around the Campbell Scientific CSAT3 sonic anemometer relative to incident wind direction. *Journal of Atmospheric and Oceanic Technology*, **26**: 582-592.
- Friehe, C. A., 1976. Effects of sound fluctuations on sonic anemometer measurements. *Journal of Applied Meteorology*, **15**: 607-610.
- Grant, A. L. M., and Watkins, R. D., 1989. Errors in turbulence measurements with a sonic anemometer. *Boundary-Layer Meteorology*, **46**: 181-194.
- Grelle, A., and Lindroth, A., 1994. Flow distortion by a Solent sonic anemometer: Wind tunnel calibration and its assessment for flux measurements over forest and field. *Journal of Atmospheric and Oceanic Technology*, **11**: 1529-1542.
- Horst, T. W., and Oncley, S. P., 2006. Corrections to inertial-range power spectra measured by CSAT3 and Solent Sonic anemometers, 1. Path-averaging errors. *Boundary-Layer Meteorology*, **119**: 375-395.
- Kaimal, J. C., and Businger, J. A., 1963. A continuous-wave sonic anemometer-thermometer. *Journal of Applied Meteorology*, **2**: 156-164.
- Kaimal, J. C., Gaynor, J. E., Zimmerman, H. A., and Zimmerman, G. A., 1990. Minimizing flow distortion errors in a sonic anemometer. *Boundary-Layer Meteorology*, **53**: 103-115.
- Kaimal, J. C., Izumi, I., and Coté, O. R., 1972. Spectral characteristics of surface layer turbulence. *Quarterly Journal of the Royal Meteorological Society*, **98**: 563-589.
- Kochendorfer, J., Meyers, T. P., Frank, J., Massman, W. J., and Heuer, M. W., 2012. How well can we measure the vertical wind speed? Implications for fluxes of energy and mass. *Boundary-Layer Meteorology*, **145**: 383-398.
- Kraan, C., and Oost, W. A., 1989. A new way of anemometer calibration and its application to a sonic anemometer. *Journal of Atmospheric and Oceanic Technology*, **6**: 516-524.
- Larsen, S. E., Edson, J. B., Fairall, C. W., and Mestayer, P. G., 1993. Measurement of temperature spectra by a sonic anemometer. *Journal of Atmospheric and Oceanic Technology*, **10**: 345-354.
- Liu, H. P., Peters, G., and Foken, T., 2001. New equations for sonic temperature variance and buoyancy heat flux with omnidirectional sonic anemometer. *Boundary-Layer Meteorology*, **100**: 459-468.
- Monin, A. S., and Obukhov, A. M., 1954. Basic laws of turbulent mixing in the surface layer of the atmosphere. *Trudy Geofizicheskogo Instituta, Akademiya Nauk SSSR*, **24**: 163-187.
- Moore, C. J., 1986. Frequency response corrections for eddy correlation systems. *Boundary-Layer Meteorology*, **37**: 17-35.
- Nakai, T., and Shimoyama, K., 2012. Ultrasonic anemometer angle attack errors under turbulent conditions. *Agricultural and Forest Meteorology*, **162-163**: 14-26.
- Schotanus, P., Nieuwstadt, F. T. M., and De Bruin, H. A. R., 1983. Temperature measurement with a sonic anemometer and its application to heat and moisture fluxes. *Boundary-Layer Meteorology*, **26**: 81-93.
- Schotland, R. M., 1955. The Measurement of wind velocity by sonic means. *Journal of Meteorology*, **12**: 386-390.
- Swinbank, W. C., 1951. The measurement of vertical transfer of heat and water vapor by eddies in the lower atmosphere. *Journal of Meteorology*, **8**: 135-145.
- van Boxel, J. H., Sterk, G., and Arens, S. M., 2004. Sonic anemometers in aeolian sediment transport research. *Geomorphology*, **59**: 131-147.
- Vellinga, O. S., Dobosy, R. J., Dumas, E. J., Gioli, B., Elbers, J. A., and Hutjes, R. W. A., 2013. Calibration and quality assurance of flux observations from a small research aircraft. *Journal of Atmospheric and Oceanic Technology*, **30**: 161-181.
- Wieser, A., Fiedler, F., and Corsmeier, U., 2001. The influence of the sensor design on wind measurements with sonic anemometer systems. *Journal of Atmospheric and Oceanic Technology*, **18**: 1585-1608.
- Wyngaard, J. C., 1981. The effects of probe-induced flow distortion on atmospheric turbulence measurements. *Journal of Applied Meteorology*, **20**: 784-794.
- Wyngaard, J. C., and Zhang, S. F., 1985. Transducer-shadow effects on turbulence spectra measured by sonic anemometers. *Journal of Atmospheric and Oceanic Technology*, **2**: 548-558.
- Zhang, J. A., 2010. Spectral characteristics of turbulence in the hurricane boundary layer over ocean between the outer rainbands. *Quarterly Journal of the Royal Meteorological Society*, **136**: 918-926.

(Edited by Xie Jun)